Ocean Systems Engineering, *Vol. 10, No. 1 (2020) 67-86*
DOI: https://doi.org/10.12989/ose.2020.10.1.067

Free vibration analysis of large sag catenary with application to catenary jumper

Karun Klaycham*[1], Panisara Nguantud[2a],
Chainarong Athisakul[2b] and Somchai Chucheepsakul[2c]

[1]*Department of Civil Engineering, Faculty of Engineering at Kamphaeng Saen, Kasetsart University, Nakhon Pathom 73140, Thailand*
[2]*Department of Civil Engineering, Faculty of Engineering, King Mongkut's University of Technology Thonburi, Bangkok 10140, Thailand*

(Received June 25, 2019, Revised November 8, 2019, Accepted November 6, 2019)

Abstract. The main goal of this study is to investigate the free vibration analysis of a large sag catenary with application to the jumper in hybrid riser system. The equation of motion is derived by using the variational method based on the virtual work principle. The finite element method is applied to evaluate the numerical solutions. The large sag catenary is utilized as an initial configuration for vibration analysis. The nonlinearity due to the large sag curvature of static configuration is taken into account in the element stiffness matrix. The natural frequencies of large sag catenary and their corresponding mode shapes are determined by solving the eigenvalue problem. The numerical examples of a large sag catenary jumpers are presented. The influences of bending rigidity and large sag shape on the free vibration behaviors of the catenary jumper are provided. The results indicate that the increase in sag reduces the jumper natural frequencies. The corresponding mode shapes of the jumper with large sag catenary shape are comprised of normal and tangential displacements. The large sag curvature including in the element stiffness matrix increases the natural frequency especially for a case of very large sag shape. Mostly, the mode shapes of jumper are dominated by the normal displacement, however, the tangential displacement significantly occurs around the lowest point of sag. The increase in degree of inclination of the catenary tends to increase the natural frequencies.

Keywords: catenary jumper; finite element method; free vibration analysis; large sag catenary; hybrid riser; natural frequency; variational method; virtual work

1. Introduction

In offshore engineering, marine riser is considered as a major structural link between the seafloor and the floating platform, i.e., spar platform and tension leg platform (Zou 2012, Ibrahim and Jameel 2018), its main function is to convey oil and gas from the wellhead to the platform. It plays a significant role in deepwater drilling and production operations for the oil and gas industry. For

*Corresponding author, Ph.D., E-mail: karun.kl@ku.ac.th
[a] Master Student, E-mail: pormanmint@hotmail.com
[b] Ph.D., E-mail: Chainarong.ath@kmutt.ac.th
[c] Professor, E-mail: Somchai.chu@kmutt.ac.th

http://www.techno-press.org/?journal=ose&subpage=7 ISSN: 2093-6702 (Print), 2093-677X (Online)

deep-water operation with harsh environmental condition near the ocean surface zone, the hybrid riser system becomes an alternative solution (Kim *et al*. 2018). For this riser system, the catenary-type configuration known as steel catenary jumper (Rombado *et al*. 2012) or conventional flexible jumper (Kim and O'Reilly 2019) can be the upper part of the free-standing hybrid riser system (Andueza *et al*. 2011, Rombado *et al*. 2012, Cao and Chen 2017, Kim *et al*. 2018, Kim and O'Reilly 2019). If this type of riser is mainly subjected to its self-weight, it can form the catenary shape with large sag curve (Athisakul *et al*. 2011, Athisakul *et al*. 2014, Klaycham *et al*. 2014). Conveniently, the catenary-type riser in large sag catenary configuration can get back to equilibrium by its self-weight if top end movement is applied (Bai 2001). In case of large sag catenary, the lowest point of the catenary curve may be not located in the same point of the bottom end support. On the contrary to the free hanging riser system, the lowest point of the riser system is the touch down point and the sag to span length ratio ($y_{smax}:L$) of the riser is limited to be less than 1:8. However, as the operations further move into the deeper water, research works which help understanding the behaviors of riser are necessary for technology development. One of the most interesting research topics is the free vibration analysis, especially when it has a very large sag configuration.

Researches on marine risers have been given attention since 1960, starting with the assumption of small displacement analysis (Graham and Frost 1965, Fischer and Ludwig 1966, Kopecky 1971, Trucker and Murtha 1973, Henghold *et al*. 1977, Chou *et al*. 1978, Dareing and Huang 1979, Krolikowski and Grey 1980, Alfosail *et al*. 2017, Su *et al*. 2018). However, in these research studies, the sag to span length ratio ($y_{smax}:L$) of the riser is limited to be less than 1:8. Many studies have examined large displacement analysis, axial deformation, and internal fluid effect (Huang, and Chucheepsakul 1985, Athisakul *et al*. 2012, Gay Neto *et al*. 2014, Wang *et al*. 2015, Adamiec-Wójcik *et al*. 2015).

Nowadays, there are few research studies concerning the large sag catenary shape analysis. Phanyasahachart *et al*. (2017) studied the static equilibrium configuration of the large sag catenary cable by using the principle of virtual work. The finite element method was used to solve the problem numerically. Their results showed that the increase in sag decreases significantly the tension force. Their model was later extended to study the free vibration behaviors of a very large sag catenary cable Phanyasahachart *et al*. (2018). They found that the free vibration behavior of very large sag cable is similar to a simple hanging chain (Huang and Dareing 1969). Although the robust mathematical model has been proposed in their study, such a model did not capture the effect of bending stiffness to provide an appropriately accurate result for the riser problem.

Therefore, this study aims to investigate the free vibration of a large sag catenary shape with application to catenary jumper for hybrid riser system. The static configuration calculated based on the catenary equation is utilized as the initial state for the vibration analysis. The variational method based on the work-energy principle is used to form the equation of motion. The finite element method along with eigenvalue problem solver is applied to obtain the numerical solutions of the natural frequencies and the vibration mode shapes. The effect of large sag catenary shape on the natural vibration behaviors of the jumper are highlighted. The bending rigidity is found to be the most significant parameter influencing on the free vibration characteristics of the jumper, especially for a large sag configuration.

2. Variational formulation for free vibration analysis of large sag catenary

Two equilibrium configurations of the catenary are shown in Figs. 1(a) and 1(b), including the static and dynamic equilibrium configurations. At the static state, the horizontal and vertical coordinates at any points of the catenary are described by x_s and y_s, respectively, in which $x_s = X_H$ and $y_s = Y_H$ at the catenary top end. The arc-length coordinate of the catenary is represented by s_s, where $s_s = 0$ at the bottom end and $s_s = S$ at the top end (S is total catenary length). The large sag static configuration (x_s and y_s) is calculated based on the catenary formula [26] as given in Appendix A. In practical design of the riser system, the most commonly used configuration for jumper is a double clamped configuration, with stress joints (for steel rigid risers) or bend stiffeners. However, in the present study, the static solution starts from the catenary formula, thus the configuration of the catenary is considered as a double pinned condition for simplicity.

As shown in Fig. 1(a), the catenary is vibrating around its static equilibrium configuration. Beyond the static state, the catenary moves to the dynamic equilibrium position, $x = x_s + u_d$ and $y = y_s + v_d$. The variables u_d and v_d are the components of dynamic displacements vector $\vec{\mathbf{u}}_d(s)$, representing horizontal and vertical displacements, respectively. Based on the differential geometry of the catenary segment, the curvature at dynamic state can be derived as the following exact formula (Chucheepsakul *et al*. 2003).

$$\kappa = x''y' - x'y'' \tag{1}$$

It should be noted that $(')$ is the differentiation with respect to the variable s_s. According to the theory of elasticity, the dynamic axial strain using the updated Lagrangian description is defined by (Chucheepsakul *et al*. 2003)

$$\varepsilon_d = \frac{s' - s'_s}{s'_s} \approx \frac{1}{s'^2_s}\left(x'_s u'_d + y'_s v'_d + \frac{u'^2_d}{2} + \frac{v'^2_d}{2} \right) \tag{2}$$

For small amplitude oscillation, the higher order terms of dynamic axial strain can be neglected, this leads to the linear dynamic axial strain as follows.

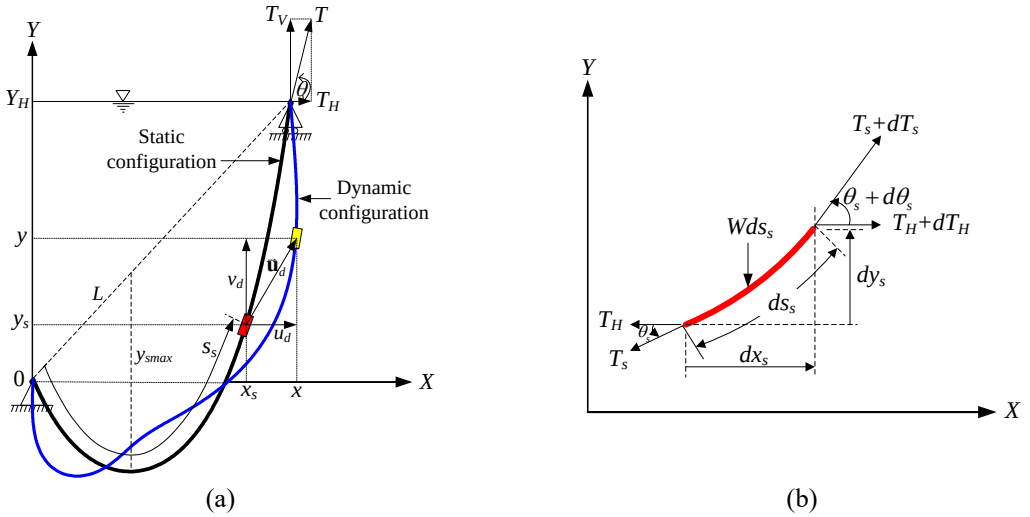

(a) (b)

Fig. 1 (a) Static and dynamic configurations of a large sag catenary and (b) Free body diagram of the catenary segment at static equilibrium state

$$\varepsilon_d \approx \frac{1}{s_s'^2}\left(x_s' u_d' + y_s' v_d'\right) \tag{3}$$

To obtain the governing equation for free vibration analysis, the variational method based on the principle of virtual displacement is applied to derive the equation of motion. The virtual strain energy comprises the axial stretching and bending. Firstly, the virtual strain energy caused by axial load can be expressed as

$$\delta U_a = \int_0^S \left(T_a x' \delta u_d' + T_a y' \delta v_d'\right) ds_s \tag{4}$$

where $T_a = T_s + EA_p\varepsilon_d$ is the axial tension at dynamic state; T_s is static axial tension calculated from Eq. (A9); and E is the modulus of elasticity. The virtual bending strain energy is given by

$$\delta U_b = \int_0^S \left(B\kappa y' \delta u_d'' - B\kappa^2 x' \delta u_d' - B\kappa x' \delta v_d'' - B\kappa^2 y' \delta v_d'\right) ds_s \tag{5}$$

where $B = EI_p$ is the flexural rigidity; and I_p is the moment of inertia. The external virtual work is performed by the effective weight and the initial force of the catenary. The virtual work done by effective weight can be expressed as

$$\delta W_W = -\int_0^S W \delta v_d ds_s \tag{6}$$

With application to jumper, $W = \left(\rho_p A_p - \rho_e A_e + \rho_i A_i\right) g$ is the effective weight; ρ_p, ρ_e and ρ_i are densities of the jumper material, sea water, and internal transported fluid, respectively; A_e, and A_i are the cross-sectional areas based on the pipe outer diameter and the pipe internal diameter, respectively, while $A_p = A_e - A_i$ is the cross-sectional area of the pipe. The virtual work caused by an initial force can be expressed as

$$\delta W_I = -\int_0^S \{(m_p + m_i + C_a^*)(\ddot{u}_d \delta u_d + \ddot{v}_d \delta v_d)\} ds_s \tag{7}$$

in which $\ddot{u}_d$ and $\ddot{v}_d$ are the horizontal and vertical accelerations of the catenary; $m_p = \rho_p A_p$ is mass per length of the catenary; $m_i = \rho_i A_i$ is mass per length of transported fluid; $C_a^* = \rho_e A_e C_a$ is the hydrodynamic added mass per unit catenary length; and C_a is the added mass coefficient. Finally, the total virtual work equation is generally written in the form

$$\delta\pi = \left(\delta U_a + \delta U_b\right) - \left(\delta W_W + \delta W_I\right) \tag{8}$$

By substituting the Eqs. (4)-(7) into Eq. (8) with some manipulations, the total virtual work functional of the catenary is

$$\begin{aligned}\delta\pi = &\int_0^S \left\{B\kappa\left(y'\right)\delta u_d'' + \left[\left(T_a - B\kappa^2\right)\left(x'\right)\right]\delta u_d' - B\kappa\left(x'\right)\delta v_d'' + \left[\left(T_a - B\kappa^2\right)\left(y'\right)\right]\delta v_d'\right\} ds_s \\ &- \int_0^S \{-\left[\left(m_p + m_i + C_a^*\right)\ddot{u}_d\right]\delta u_d - \left[\left(m_p + m_i + C_a^*\right)\ddot{v}_d + W\right]\delta v_d\} ds\end{aligned} \tag{9}$$

Eq. (9) is a nonlinear equation, which is difficult to be solved by an analytical method. Therefore,

the numerical method based on the finite element technique is utilized for solving the free vibration analysis of a large sag configuration of the catenary including nonlinear term of the static curvature. This study focuses on the free vibration of the large sag catenary shape. Consequently, only virtual work done by effective weight is included in the formulation. However, the present model formulation can be further extended to accommodate the currents loads as proposed by Athisakul *et al*. (2011), Klaycham *et al*. (2018).

3. Numerical approach

To find the solution of Eq. (9), the finite element procedure is utilized to obtain the numerical results, as more detailed procedures are given in the following subsection.

3.1 Finite element method

The finite element method is applied to evaluate the numerical solutions of the vibration analysis. In the present finite element model, the catenary is discretized into a finite number of the elements along the arc-length coordinate. To this end, the length of each discretized element of the catenary is

$$s_e = \frac{S}{n} \tag{10}$$

where S is total arc-length of the catenary, while n is the number of the finite element. The dynamic displacement of the catenary can be calculated approximately by (Monprapussorn *et al*. 2007)

$$\{\mathbf{u}_d\} = \{u_d \quad v_d\}^T \approx [\mathbf{N}]\{\mathbf{d}_n\} \tag{11}$$

in which $[\mathbf{N}]$ is the shape function matrix containing the set of fifth-degree polynomial function N_{5i} (Athisakul *et al*. 2011).

$$[\mathbf{N}] = \begin{bmatrix} N_{51} & N_{52} & N_{53} & 0 & 0 & 0 & N_{54} & N_{55} & N_{56} & 0 & 0 & 0 \\ 0 & 0 & 0 & N_{51} & N_{52} & N_{53} & 0 & 0 & 0 & N_{54} & N_{55} & N_{56} \end{bmatrix} \tag{12}$$

and $\{\mathbf{d}_n\}$ is the nodal degree of freedom vector representing nodal dynamic displacements and their derivatives.

$$\{\mathbf{d}_n\} = \{u_{1d} \quad u'_{1d} \quad u''_{1d} \quad v_{1d} \quad v'_{1d} \quad v''_{1d} \quad u_{2d} \quad u'_{2d} \quad u''_{2d} \quad v_{2d} \quad v'_{2d} \quad v''_{2d}\}^T \tag{13}$$

3.2 Equation of motion

Based on the virtual work principle, the dynamic equilibrium equation of the catenary is derived by applying the stationary condition to Eq. (9). In addition, according to the finite element procedure, substituting Eq. (11) into Eq. (9) leads to the element equation of motion in a matrix form as

$$\left[\mathbf{m}^{(e)}\right]\{\ddot{\mathbf{d}}_n\} + \left[\mathbf{k}^{(e)}\right]\{\mathbf{d}_n\} = \{\mathbf{0}\} \tag{14}$$

in which $\left[\mathbf{m}^{(e)}\right]$ is the element mass matrix as given by

$$\left[\mathbf{m}^{(e)}\right] = \int_0^{s_e} \left\{ \left(m_p + m_i + C_a^*\right)[\mathbf{N}]^T \begin{bmatrix} 1 & 0 \\ 0 & 1 \end{bmatrix} [\mathbf{N}] \right\} ds_s \tag{15}$$

$[\mathbf{k}^{(e)}]$ is the element stiffness matrix including of

$$\left[\mathbf{k}^{(e)}\right] = \left[\mathbf{k}_{b1}^{(e)}\right] + \left[\mathbf{k}_{b2}^{(e)}\right] + \left[\mathbf{k}_{t1}^{(e)}\right] \tag{16}$$

where $[\mathbf{k}_{b1}^{(e)}]$ and $[\mathbf{k}_{b2}^{(e)}]$ are the bending stiffness matrices. The matrix $[\mathbf{k}_{t1}^{(e)}]$ is the stiffness matrix resisting axial deformation.

$$\left[\mathbf{k}_{b1}^{(e)}\right] = \int_0^{s_e} B[\mathbf{N}'']^T \begin{bmatrix} y_s'^2 & -x_s' y_s' \\ -x_s' y_s' & x_s'^2 \end{bmatrix} [\mathbf{N}''] ds_s \tag{17}$$

$$\left[\mathbf{k}_{b2}^{(e)}\right] = \int_0^{s_e} \left\{ B\kappa_s [\mathbf{N}']^T \begin{bmatrix} 2x_s' y_s' & y_s'^2 - x_s'^2 \\ y_s'^2 - x_s'^2 & -2x_s' y_s' \end{bmatrix} [\mathbf{N}''] \right\} ds_s \tag{18}$$

$$\left[\mathbf{k}_{t1}^{(e)}\right] = \int_0^{s_e} \left\{ [\mathbf{N}']^T \begin{bmatrix} T_s & 0 \\ 0 & T_s \end{bmatrix} [\mathbf{N}'] + EA_p [\mathbf{N}']^T \begin{bmatrix} x_s'^2 & x_s' y_s' \\ x_s' y_s' & y_s'^2 \end{bmatrix} [\mathbf{N}'] \right\} ds_s \tag{19}$$

where T_s is the static axial tension, which can be obtained from Eq. (A9). The variables x_s' and y_s' in Eqs. (17)-(19) can be derived from the exact catenary formula by differentiating Eqs. (A6) and (A7) with respect to s_s.

$$x_s' = \left[\left(\frac{W s_s}{T_H} + \sinh K_1 \right)^2 + 1 \right]^{-\frac{1}{2}} \tag{20}$$

$$y_s' = \left\{ \sinh\left[\sinh^{-1}\left(\frac{W s_s}{T_H} + \sinh K_1 \right) \right] \right\} \left(\frac{W s_s}{T_H} + \sinh K_1{}^2 + 1 \right)^{-\frac{1}{2}} \tag{21}$$

In the same manner, differentiation of Eq. (A8) with respect to s_s leads to the exact expression for large curvature of the catenary, $\kappa_s = d\theta_s / ds_s$, as

$$\kappa_s = \frac{W}{T_H} \cdot \frac{\left\{ \cosh\left[\sinh^{-1}\left(\frac{W s_s}{T_H} + \sinh K_1 \right) \right] \right\} \left[\left(\frac{W s_s}{T_H} + \sinh K_1 \right)^2 + 1 \right]^{-\frac{1}{2}}}{1 + \left\{ \sinh\left[\sinh^{-1}\left(\frac{W s_s}{T_H} + \sinh K_1 \right) \right] \right\}^2} \tag{22}$$

The element equation of motion from Eq. (14) is assembled to obtain the equation of motion of the global system.

$$[\mathbf{M}]\{\ddot{\mathbf{D}}_n\} + [\mathbf{K}]\{\mathbf{D}_n\} = \{\mathbf{0}\} \tag{23}$$

where $\{\mathbf{D}_n\} = \sum_{i=1}^{n}\{\mathbf{d}_n\}$ and $\{\ddot{\mathbf{D}}_n\} = \sum_{i=1}^{n}\{\ddot{\mathbf{d}}_n\}$ are the global nodal displacement and nodal acceleration vectors, respectively; $[\mathbf{M}] = \sum_{i=1}^{n}\left[\mathbf{m}^{(e)}\right]$ is the total mass matrix; and $[\mathbf{K}] = \sum_{i=1}^{n}\left[\mathbf{k}^{(e)}\right]$ is the total stiffness matrix. For free vibration, the general solution is a harmonic function, therefore Eq. (23) leads to the eigenvalue problem in the form as

$$\left([\mathbf{K}] - \omega^2[\mathbf{M}]\right)\{\bar{\mathbf{D}}\} = \{\mathbf{0}\} \tag{24}$$

in which ω and $\{\bar{\mathbf{D}}\}$ are the natural frequencies and vibration mode shapes of the catenary obtained by solving the eigenvalue problem, Eq. (24). In this study, for more convenience, the computer program is developed by using the Fortran-90 language to implement the finite element algorithm and the eigenvalue problem solver.

4. Numerical results and application to catenary jumper

In this section, the numerical examples with the application to large sag catenary jumper are presented. The effect of bending rigidity and large sag configuration on the natural frequencies and the vibration mode shapes are investigated.

4.1 Numerical validations

As the mathematical model and computer code are developed for implementing the finite element algorithm, its numerical accuracy needs to be checked. The first validation example investigates the natural frequencies of inclined taut cables, which are compared with the results presented by Henghold *et al*. (1977). To perform the present finite element simulation of the cable problem, the bending stiffness is neglected. The cable stiffness to weight ratio (EA/WS) is specified to be 5000 with two different inclined angles of 30 and 60 degrees. The other input parameters of cable are shown in Table 1, while the comparison of dimensionless natural frequencies of cable ($\hat{\omega} = \omega\sqrt{S/g}$) are demonstrated in Table 2. It is revealed that, in the case of inclined cable, the present natural frequencies are acceptable with those results present by Henghold *et al*. (1977). However, their maximum differences are 3% and 5% for the inclined angle of 30 and 60 degrees, respectively. These differences may be caused by unequal number of the discretized element.

In addition to inclined taut cable, the natural frequencies of the large sag horizontal cable suspended in the air are also investigated, which are compared with those results presented by Phanyasahachart *et al*. (2018). In this validation example, the properties of the cable are shown in Table 3. Two different values of horizontal top tensions are examined such as 10 N and 1500 N. The comparisons between natural frequencies for the first four vibration modes are shown in Table 4. From the comparisons, good agreement can be found with results presented by Phanyasahachart *et al*. (2018).

Maximum differences of 6.5% and 0.5% can be found for T_H = 10 N and 1500 N.

Table 1 Parameters of the inclined cables

Input variables	Inclined angle (degrees)	
	30	60
Horizontal top tension, T_H (kN)	6320	3840
Total arc-length, S (m)	1038	1798
Diameter, D (m)	0.3842	0.3842
Cable weight in air, W (kN/m)	9.48	9.48
Modulus of elasticity, E (kN/m^2)	4.25 x 10^8	7.353 x 10^8

Table 2 Comparisons of dimensionless natural frequencies for the first two vibration modes of inclined taut cables

Mode	Dimensionless Frequencies, $\hat{\omega} = \omega\sqrt{S/g}$			
	Inclined 30 degrees		Inclined 60 degrees	
	This study	Henghold *et al*. (1977)	This study	Henghold *et al*. (1977)
1	5.14	5.17	3.84	3.65
2	7.90	8.17	6.32	6.30

Table 3 Parameters of the cables

Input variables	Values
Horizontal top tension, T_H (N)	10, 1500
Total arc-length, S (m)	869.42
Diameter, D (m)	0.023
Cable weight in air, W (N/m)	9.48
Modulus of elasticity, E (kN/m^2)	1.794 x 10^9

Table 4 Comparison of the natural frequencies for the first four vibration modes of the large sag horizontal cables

Mode	Natural frequencies (rad/s)			
	T_H = 10 N		T_H = 1500 N	
	This study	Phanyasahachart *et al*. (2018)	This study	Phanyasahachart *et al*. (2018)
1	0.1852	0.1814	0.2683	0.2678
2	0.2728	0.2809	0.4796	0.4790
3	0.4508	0.4247	0.6791	0.6785
4	0.5594	0.5739	0.8692	0.8683

Table 5 Parameters of the jumper and environmental conditions

Parameters	Values
Total arc-length, S (m)	1000
Number of discretization, n	40
Outer diameter, D_e (m)	0.26
Inner diameter, D_i (m)	0.20
Modulus of elasticity, E (N/m^2)	2.07 x 10^{11}
Densities of pipe, ρ_p, sea water, ρ_e, and internal fluid, ρ_i (kg/m^3)	7850, 1025, 998
Added mass coefficient, C_a	1.0

4.2 Effect of bending stiffness on free vibration of jumper with large sag configuration

This subsection presents the effect of bending stiffness on the free vibration characteristics of a jumper. The properties of the horizontal jumper and ocean conditions are given in Table 5. The total length of the jumper is 1000 m. Fig. 2 show the relation between the first fundamental frequency and horizontal top tension (T_H), for the including (IBS) and excluding bending stiffness (EBS) of the jumper in the numerical computation cases. From Fig. 2(a), for a small value of T_H, the catenary has a large sag curve. If the value of T_H is increased, the catenary has a rather taut static configuration, and increased its natural frequency as well.

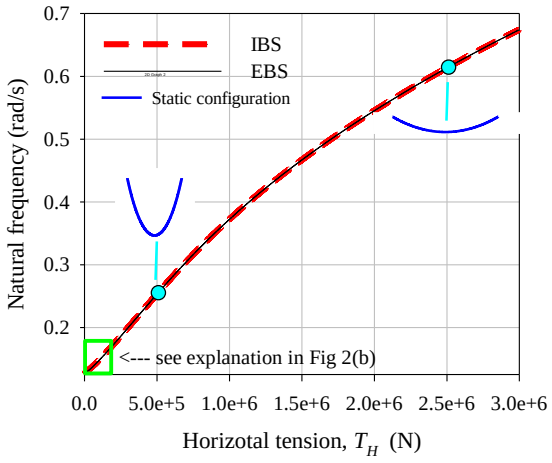

(a) Natural frequency versus horizontal top tension

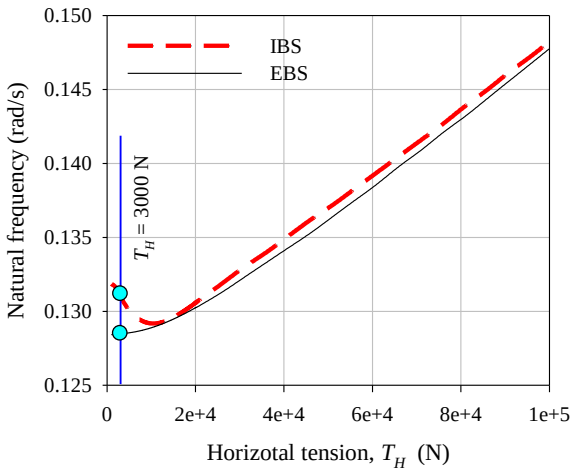

(b) Natural frequency versus horizontal top tension (Explanation from Fig. 2(a))

Fig. 2 Effect of bending rigidity on the natural frequency of a jumper: abbreviations "IBS" and "EBS" represent the including and excluding bending stiffness, respectively

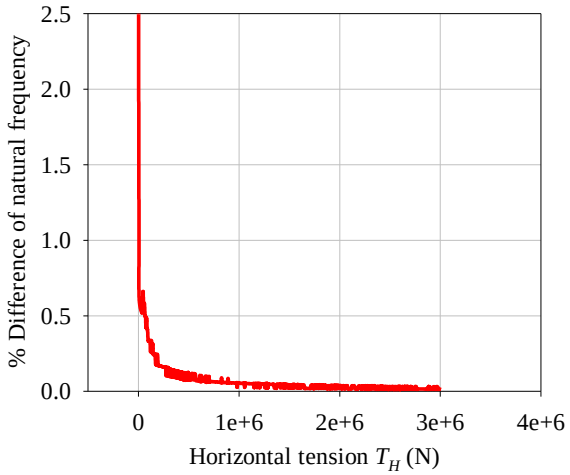

Fig. 3 Percent difference of the natural frequency of a jumper obtained by including and excluding bending stiffness ("IBS" and "EBS")

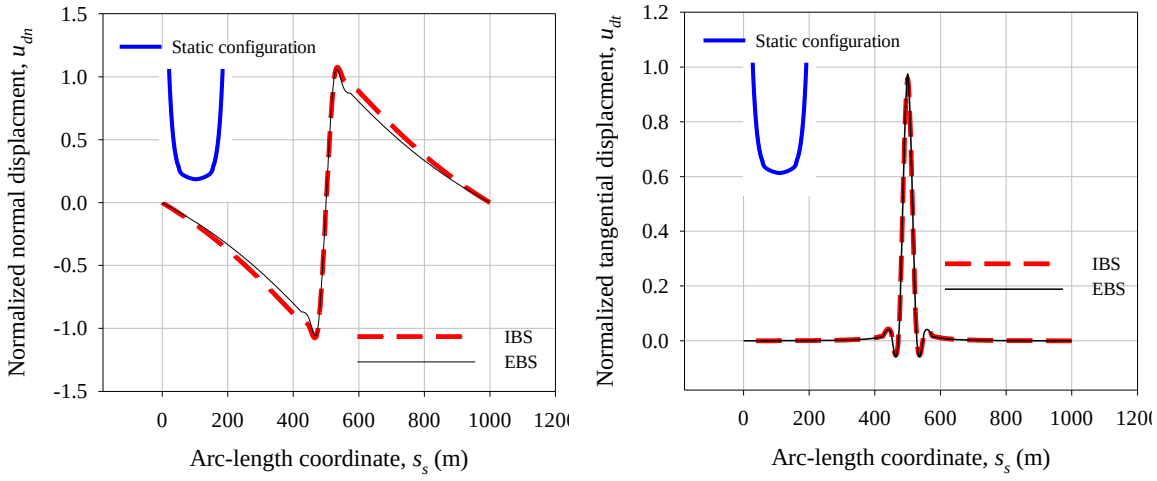

(a) Normalized normal displacements (b) Normalized tangential displacement

Fig. 4 First fundamental mode shapes of a catenary, for horizontal top tension of T_H = 3000 N, in comparing between including bending stiffness (IBS) and excluding bending stiffness (EBS)

For a small value of T_H (large sag configuration), the bending stiffness contributes more to the dynamic characteristics as seen from the explanation in Fig. 2(b)). This result is also shown in Fig. 3, where the percent difference in natural frequency obtained by including and excluding bending stiffness in the computation is illustrated. Fig. 3 reveals that, for a taut and straight jumper (large value of T_H), the free vibration behavior of a catenary is dominated by axial tension and the bending stiffness has an insignificant influence on free vibration behavior.

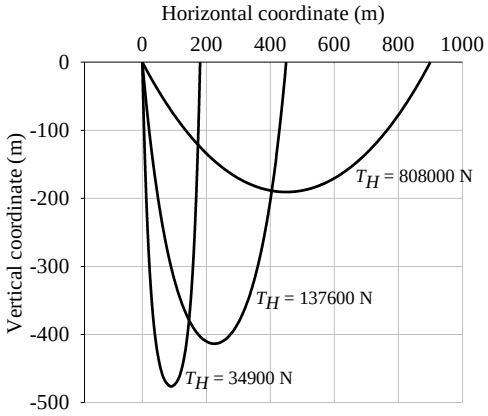

Fig. 5 Static configurations of horizontal jumpers for different horizontal top tensions

Considering the effect of bending stiffness on fundamental mode shape (see Fig. 4) for T_H = 3000 N, the modal displacement in normal (u_{dn}) and tangential (u_{dt}) directions are shown in Figs. 4(a) and 4(b), respectively, which can be calculated as follows

$$u_{dn} = u_d \sin\theta_s - v_d \cos\theta_s \tag{25}$$

$$u_{dt} = u_d \cos\theta_s + v_d \sin\theta_s \tag{26}$$

where θ_s is the angle measured from horizontal direction to the tangential direction of jumper as calculated from Eq. (A8). The result shows that the bending stiffness is insignificant on fundamental tangential displacement mode since the mode shape of IBS looks identical to that of EBS, as seen in Fig. 4(b). However, the bending stiffness has significantly more influence on fundamental normal displacement mode.

4.3 Free vibration of horizontal jumper

The propose of this subsection is to present the effect of horizontal top tension (T_H) on the free vibration behavior of the horizontal jumper. The parameters of the jumper and environmental condition used in this study are given in Table 5. As the horizontal jumper is investigated in this subsection, therefore the supports of the jumper are placed at the same level (Y_H = 0). The total arc-length of 1000 m is specified, while three different values of the horizontal top tension such as T_H =34900 N, 137600 N, and 808000 N are investigated. It should be noted that, in case of T_H ==34900 N, although this value of horizontal tension at top end (T_H) is small, the top tension along the tangential direction is large enough to carry its self-weight.

The static configurations of a large sag catenary jumper for different horizontal top tensions are shown in Fig. 5. As three different horizontal top tension of 34900 N, 137600 N, and 808000 N are specified, the corresponding horizontal offset calculated from Eq. (A7) are found to be 180.0 m, 450.0 m, and 900.0 m, respectively. This means that the effect of horizontal top tension is to move horizontally the right end of jumper away from the other end, and to decrease the sag to span length

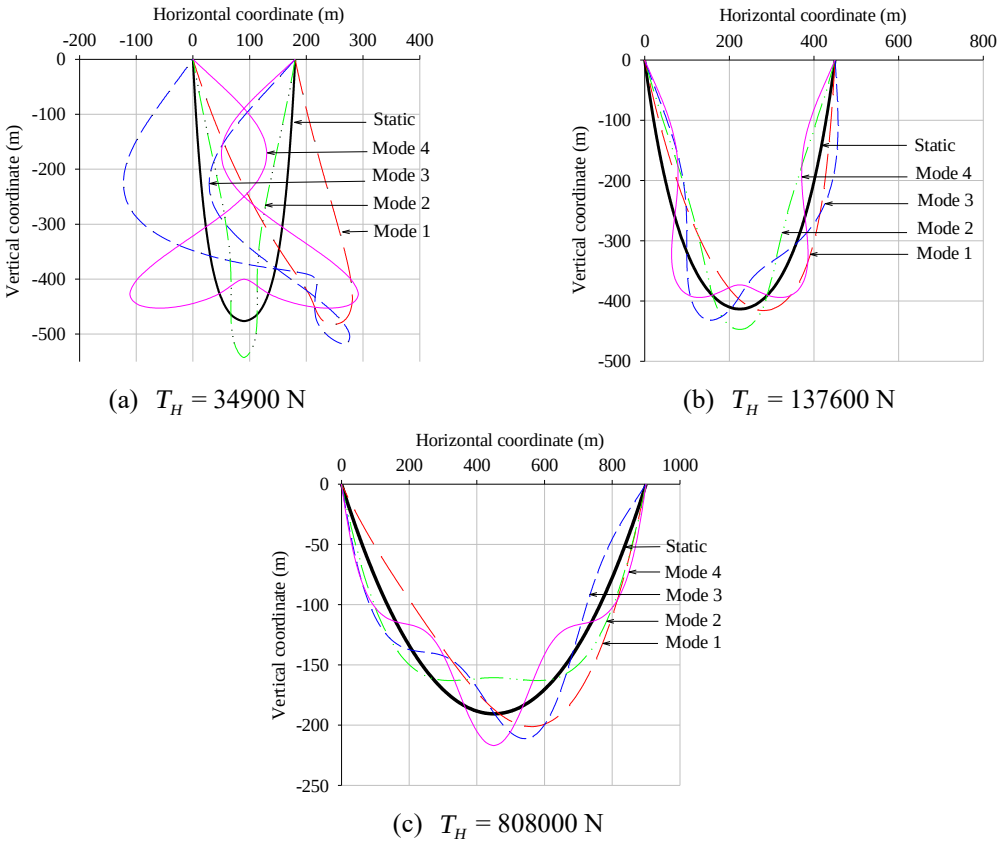

(a) T_H = 34900 N (b) T_H = 137600 N

(c) T_H = 808000 N

Fig. 6 Static and modal dynamic configurations of horizontal jumper

ratio. This result is also graphically confirmed by Fig. 5. The numerical value of the sag to span length ratios for their corresponding horizontal tensions are given in Table 6. It also shows the natural frequencies for the first four vibration modes of the jumper. It is shown that the increase in horizontal top tensions also increases the natural frequency of the jumper. This result is due to the horizontal top tension directly increasing the jumper stiffness (see Eqs. (A9) and (19)), which increases natural frequencies as well. If the horizontal top tension is large enough, the sag to span length ratio ($y_{smax} : L$) is very small; therefore the natural frequency of the horizontal jumper is mainly dominated by axial stiffness, and could approach the solution of a classical vibrating string problem.

The static and the modal dynamic configurations (first four modes) are presented in Fig. 6. It should be noted that the modal dynamic configurations are calculated by adding the scaled normalized modal dynamic displacement (mode shape) into the static coordinate. As can be seen from Figs. 6(a)-(c), the modal dynamic configurations of jumper with large sag shape are asymmetric for odd modes (1st and 3rd modes), and symmetric for even modes (2nd and 4th modes). Fig. 7 shows the relation between the natural frequencies for the first four vibration modes and the horizontal top tension. The modal displacement in normal (u_{dn}) and tangential (u_{dt}) directions, which can be calculated from Eqs. (25) and (26), are also attached in Figs. 7(a) and 7(b), respectively.

Table 6 Natural frequencies of horizontal jumper for different horizontal top tensions

Mode	Natural Frequencies (rad/s)		
	T_H = 34900 N	T_H = 137600 N	T_H = 808000 N
Sag : Span	1 : 0.379	1 : 1.11	1 : 4.72
1	0.1336	0.1574	0.3301
2	0.2230	0.2828	0.5241
3	0.3392	0.4120	0.7279
4	0.4517	0.5364	0.9141

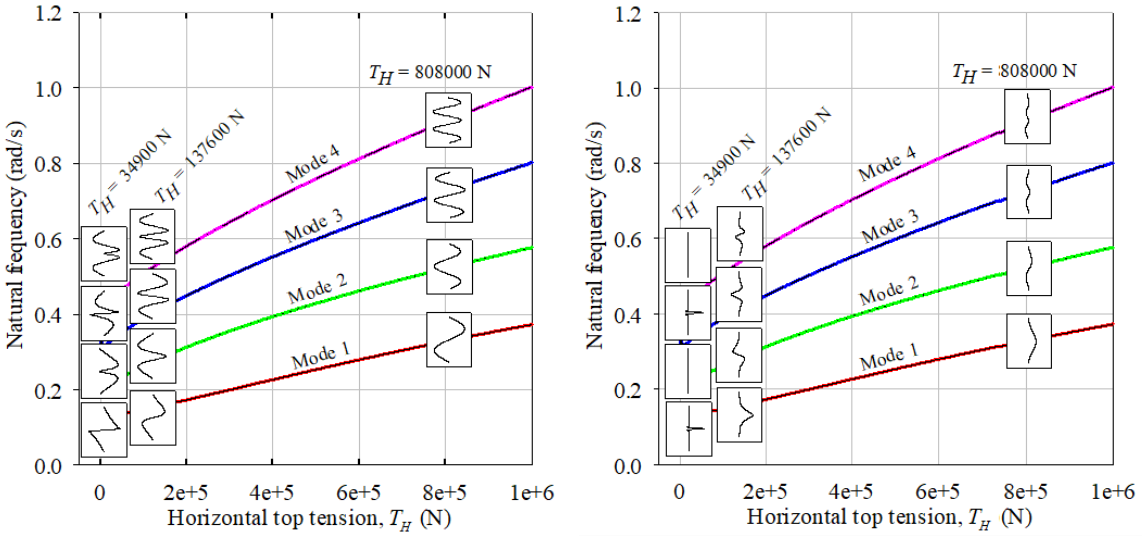

(a) Modal normal displacements (b) Modal tangential displacements

Fig. 7 Relations between the natural frequency for the first four vibration modes and the horizontal top tension of horizontal jumper

The results also confirm that the increase in horizontal top tension increases the natural frequency of the horizontal jumper. In addition, the numerical results show that the mode shapes are always dominated by normal displacement. However, the lowest point of sag in odd modes are noticeably influenced by tangential displacement, whereas the lowest point of sag in even modes are influenced by normal displacement.

4.4 Free vibration of inclined jumper

The free vibration response of the inclined jumper is presented in this subsection. The parameters of the jumper and environmental conditions given in Table 5 are used. Two different values of the vertical distance, 500 m and 866 m, are considered. For each vertical distance, three values of horizontal top tensions such as 3500 N, 137600 N, and 808000 N are applied at the top of the jumper.

Table 7 Natural frequencies of inclined jumper

Mode	Natural Frequencies (rad/s)					
	T_H = 3500 N		T_H = 137600 N		T_H = 808000 N	
	Y_H =500 m	Y_H =866 m	Y_H =500 m	Y_H =866 m	Y_H =500 m	Y_H =866 m
Sag : Span	1 : 0.79	1 : 1.16	1 : 1.58	1 : 2.54	1 : 5.50	1 : 9.28
1	0.1265	0.1275	0.1604	0.1892	0.3572	0.4835
2	0.2308	0.2521	0.2990	0.3508	0.5581	0.7149
3	0.3361	0.3667	0.4320	0.5083	0.7780	1.0060
4	0.4529	0.4946	0.5646	0.6622	0.9747	1.2370

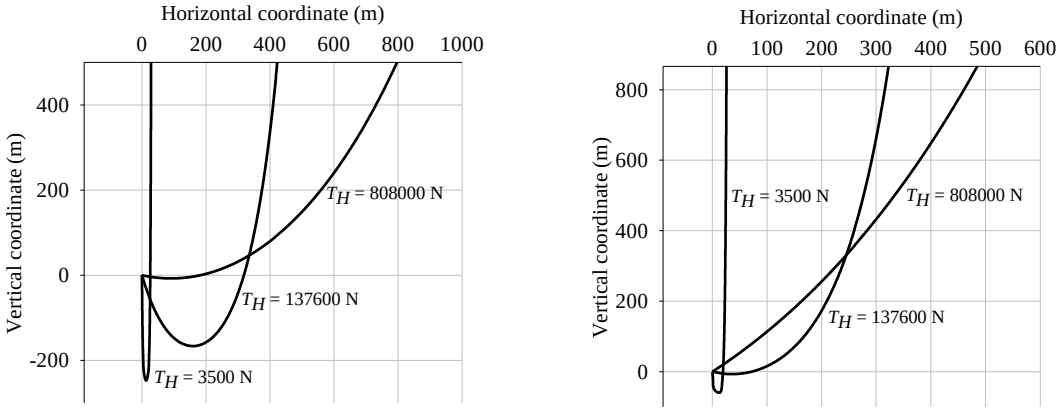

(a) Vertical distance of 500 m (b) Vertical distance of 866 m

Fig. 8 Static configurations of inclined jumpers for different horizontal top tensions

The static configurations of the inclined jumper, for vertical distances of 500 and 866 m, are illustrated in Figs. 8(a) and 8(b), respectively. This figure shows that the inclined jumper has a large sag to span length ratio ($y_{smax} : L$) when the horizontal top tension and the vertical distance are small. The natural frequencies for the first four vibration modes of the inclined jumper and the values of sag to span length ratios are shown in Table 7. This table shows that both increases in the horizontal top tension and the vertical distance decrease sag to span length ratio, and cause to increase the natural frequencies of the jumper. These results are found to be in agreement with the results for the horizontal jumper shown in the previous subsection.

To demonstrate the modal dynamic configuration of the inclined jumper, only the 500 m vertical distance case is presented, as shown in Fig. 9. As for the results, the modal dynamic configurations for the inclined jumper seem to be a fraction of those for the horizontal jumper. Fig. 10 shows the relations between the natural frequency (first four vibration modes) and the horizontal top tension of inclined jumper for the vertical distance of 500 m. The dynamic displacement (mode shape) in normal and tangential directions are also attached in Figs. 10(a) and 10(b), respectively. From this figure, the similar results with the case of horizontal jumper can be found, where the horizontal top tension increases the natural frequency of the jumper.

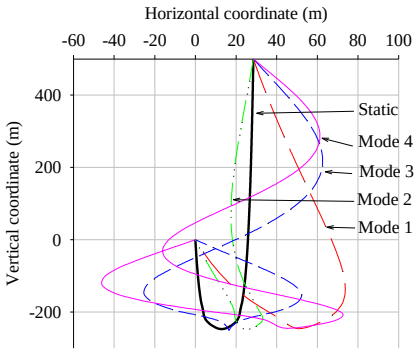

(a) T_H = 3500 N

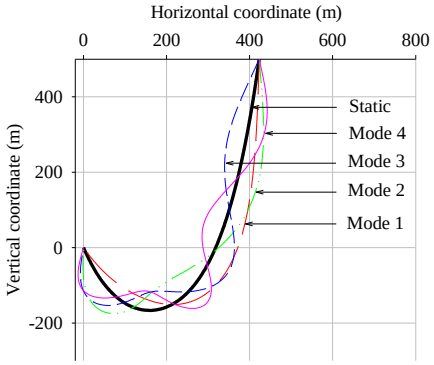

(b) T_H = 137600 N

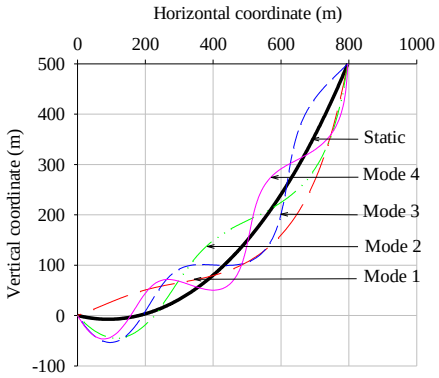

(c) T_H = 808000 N

Fig. 9 Static and modal dynamic configurations of the inclined jumper for the vertical distance of 500 m

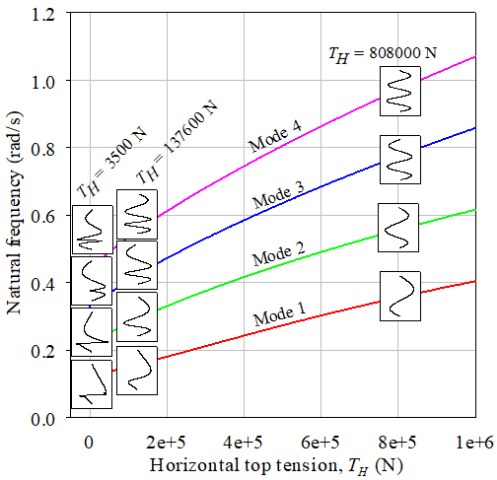

(a) Modal normal displacements

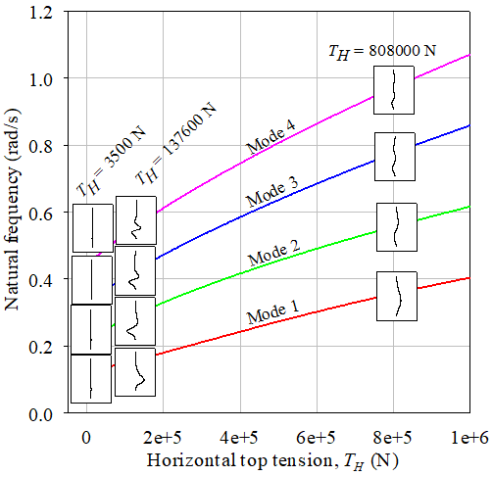

(b) Modal tangential displacements

Fig. 10 Relations between the natural frequency for the first four vibration modes and the horizontal top tension of inclined jumper for the vertical distance of 500 m

5. Conclusions

The free vibration analysis of a large sag catenary shape with application to catenary jumper in hybrid riser system is presented in this paper. The equation of motion is derived by using the variational method based on the virtual work principle. The bending stiffness of the large sag configuration is also included in the element stiffness matrix. The finite element method with the incorporated eigenvalue problem solver is used to find the natural frequencies and the vibration mode shapes. Good agreement can be found from the numerical comparisons of a large sag cable problem with the literature. Two particular jumper configurations are parametrically investigated, including horizontal and inclined jumpers, which can contribute as a benchmark solution. The numerical results reveal that the corresponding mode shapes of the jumper with large sag static configuration are comprised of normal and tangential displacements. In general, the normal displacement dominates the mode shape of a large sag catenary jumper. However, at the lowest point of sag, the tangential displacement is significant. The increase in inclination increases the natural frequency of the inclined large sag catenary. The increase in sag reduces the natural frequencies of large sag catenary. The bending stiffness increases the natural frequency, especially for very large sag shape case.

Acknowledgments

The authors would like to acknowledge the Institutional research Capability Development Grant from Thailand Research Fund (TRF) and King Mongkut's University of Technology Thonburi (KMUTT).

References

Adamiec-Wójcik, I., Brzozowska, L. and Drąg, L. (2015), "An analysis of dynamics of risers during vessel motion by means of the rigid finite element method", *Ocean Eng.*, **106**, 102-114. https://doi.org/10.1016/j.oceaneng.2015.06.053.

Alfosail, F.K., Nayfeh, A.H. and Younis, M.I. (2017), "Natural frequencies and mode shapes of statically deformed inclined risers", *J. Non-Linear Mech.*, **94**, 12-19. https://doi.org/10.1016/j.ijnonlinmec.2016.09.007.

Andueza, A., Estefen, S.F. and Marques, da Silva, R. (2011), "Steel hybrid riser for water depths up to 3000 meters", *International Conference on Offshore Mechanics and Arctic Engineering*, Rotterdam, Netherlands, June.

Athisakul, C., Monprapussorn, T. and Chucheepsakul, S. (2011), "A Variational formulation for three-dimensional analysis of extensible marine riser transporting fluid", *Ocean Eng.*, **38**(4), 609-620. https://doi.org/10.1016/j.oceaneng.2010.12.012.

Athisakul, C., Klaycham, K., Phanyasahachart, T., and Chucheepsakul, S. (2011), "Critical Top Tension of an Extensible Catenary Riser", *Proceedings of the 21st International Offshore and Polar Engineering Conference*, Hawaii, USA, June.

Athisakul, C., Phanyasahachart, T., Klaycham, K. and Chucheepsakul, S. (2012), "Static Equilibrium Configurations and Appropriate Applied Top Tension of Extensible Marine Riser with Specified Total Arc-Length using Finite Element Method", *Eng. Struct.*, **34**, 271-277. https://doi.org/10.1016/j.engstruct.2011.08.031.

Athisakul, C., Klaycham, K. and Chucheepsakul, S. (2014), "Critical top tension for static equilibrium configuration of a steel catenary riser", *China Ocean Eng.*, **28**(6), 829-842. https://doi.org/10.1007/s13344-

014-0064-x.
Bai, Y. (2001), *Pipelines and Risers*, Elsevier Science Ltd, Amsterdam, North Holland, Netherlands.
Cao, Y. and Chen, H. (2017), "CFD simulation of vortex-induced vibration of free-standing hybrid riser", *Ocean Syst. Eng.*, **7**(3), 195-223. https:// doi.org/10.12989/ose.2017.7.3.195.
Chou, D.Y., Minner, W.E., Ragusa, L. and Ho, R.T. (1978), "Dynamic analysis of couple OTEC platform cold-water pipe system", *Proceedings of Offshore Technology Conference*, Houston, U.S.A., May.
Chucheepsakul, S., Monprapussorn, T. and Huang, T. (2003), "Large strain formulations of extensible flexible marine pipes transporting fluid", *J. Fluid. Struct.*, **17**(2), 185-224. https://doi.org/10.1016/S0889-9746(02)00116-0.
Dareing, D.W. and Huang, T. (1979), "Marine riser vibration response determined by modal analysis", *J. Energy Resour. Technol.*, **101**(3), 159-166. doi:10.1115/1.3446914.
Dean, D.L. (1962), "Static and dynamic analyses of guy cables", *J. Struct. Div.- ASCE*, **127**, 382-402.
Fischer, W. and Ludwig, M. (1966), "Design of floating vessel drilling risers", *J. Petro. Tech.*, **3**(1), 272-283. https://doi.org/10.2118/1220-PA.
Gay Neto, A., Martins, C.A. and Pimenta, P.M. (2014), "Static analysis of offshore risers with a geometrically-exact 3d beam model subjected to unilateral contact", *Comput. Mech.*, **53**(1), 125-145. https://doi.org/10.1007/s00466-013-0897-9.
Graham, R.D. and Frost, M.A. (1965), "Analysis of the motion of deep-water drill string-part 1: forced lateral motion – and part 2: forced rolling motion", *J. Eng. Ind.*, **10**(2), 137-147. doi:10.1115/1.3670778.
Henghold, W.M., Russell, J.J. and Morgan, J.D. (1977), "Free vibrations of cable in three dimensions", *J. Struct. Div.- ASCE*, **103**(5), 1127-1136.
Huang, T. and Dareing, D.W. (1969), "Frequencies of a hanging chain", *J. Acoust. Soc. Am.*, **45**, 1046-1049. https://doi.org/10.1121/1.1911505.
Huang, T. and Chucheepsakul, S. (1985), "Large displacement analysis of a marine riser", *J. Energy Resour. Technol.*, **107**(1), 54-59. doi:10.1115/1.3231163.
Ibrahim, A.E. and Jameel, M. (2018), "Wind induced response of spar-mooring-riser system", *KSCE J. Civ. Eng.*, **22**(8), 2653-2663. https://doi.org/10.1007/s12205-017-1914-x.
Kim, K.S., Choi H.S. and Kim, K.S. (2018), "Preliminary optimal configuration on free standing hybrid riser", *Int. J. Nav. Archit. Ocean Eng.*, **10**(3), 250-258. https://doi.org/10.1016/j.ijnaoe.2017.10.012.
Kim, H.T. and O'Reilly, O.M. (2019), "Instability of catenary-type flexible risers conveying fluid in subsea environments", *Ocean Eng.*, **173**, 98-115. https://doi.org/10.1016/j.oceaneng.2018.12.042.
Klaycham, K., Athisakul, C. and Chucheepsakul, S. (2014), "Nonlinear Free Vibration of a Steel Catenary Riser", *Proceedings of the 24th International Offshore and Polar Engineering Conference*, Busan, Korea, June.
Klaycham, K., Athisakul, C. and Chucheepsakul, S. (2018), "Large Amplitude Motions of Deepwater Marine Riser Transporting Fluid", *Proceedings of the 28th International Offshore and Polar Engineering Conference*, Sapporo, Japan, June.
Kopecky, J.A. (1971), "Drilling riser stress measurements", *J. Eng. Ind.*, **93**(4), 1203-1208. doi:10.1115/1.3428063.
Krolikowski, L.P. and Grey, T.A., (1980), "An improved linearization technique for frequency domain riser analysis", *Offshore Technol.*, **1**, 3777-3783. https://doi.org/10.4043/3777-MS.
Monprapussorn, T., Athisakul, C. and Chucheepsakul, S. (2007), "Nonlinear vibrations of an extensible flexible marine riser carrying a pulsatile flow", *J. Appl. Mech.*, **74**(4), 754-769. doi:10.1115/1.2711226.
Phanyasahachart, T., Athisakul, C. and Chucheepsakul, S. (2017), "Analysis of large-sag extensible catenary with free horizontal sliding at one end by variational approach", *Int. J. Struct. Stability. Dyn.*, **17**(7), 1-17, 2017. https://doi.org/10.1142/S0219455417500705.
Phanyasahachart, T., Athisakul, C. and Chucheepsakul, S. (2018), "Natural frequencies of a very large-sag extensible cable", *J. Eng. Mech.*, **144**(2), 06017020. https://doi.org/10.1061/(ASCE)EM.1943-7889.0001409.
Rombado, G. Yue, B. and Rueda, C. (2012) "Steel catenary jumper for single hybrid riser in deepwater applications", *Proceedings of the Offshore Technology Conference*, Houston, Texas, USA, April.

Su, K., Butt, S., Yang, J. and Qiu, H. (2018), "Coupled dynamic analysis for the riser-conductor of deepwater surface BOP drilling system", *J. Shock Vib.*, **2018**, 6568537. https://doi.org/10.1155/2018/6568537.

Trucker, T.C. and Murtha, J.P. (1973), "Nondeterministic analysis of a marine riser", *Proceeding of the Offshore Technology Conference*, Houston, U.S.A., May.

Wang, J., Duan, M. and Luo, J. (2015), "Mathematical model of steel lazy-wave riser abandonment and recovery in deepwater", *Mar. Struct.*, **41**, 127-153. https://doi.org/10.1016/j.marstruc.2015.02.002.

Zou, J. (2012), "Semisubmersible platforms with steel catenary risers for Western Australia and Gulf of Mexico", *Ocean Syst. Eng.*, **2**(2), 99-113. http://dx.doi.org/10.12989/ose.2012.2.2.099.

MK

Appendix A : Large sag catenary configuration

From the catenary equation, the general solution of the vertical coordinate (y_s) of catenary can be written in terms of horizontal coordinate (x_s) as follows (Dean 1962).

$$y_s = \frac{T_H}{W}\cosh\left(\frac{W}{T_H}x_s + K_1\right) + K_2 \tag{A1}$$

where T_H is the horizontal top tension; W is the effective weight of catenary. To obtain two constant parameters of integration, K_1 and K_2, two boundary conditions of the catenary are necessary, i.e., at the bottom end $x_s = 0, y_s = 0$ and at the top end $x_s = X_H$, $y_s = Y_H$. By imposing the boundary conditions to Eq. (A1), one obtains the constant parameters K_1 and K_2.

$$K_1 = \sinh^{-1}\left\{W Y_H \cdot \left[2T_H \sinh\left(\frac{W X_H}{2T_H}\right)\right]^{-1}\right\} - \frac{W X_H}{2T_H} \tag{A2}$$

$$K_2 = -\frac{T_H}{W}\cosh K_1 \tag{A3}$$

The arc-length coordinate of catenary can be expressed in terms of x_s as

$$s_s = \frac{T_H}{W}\left\{\sinh\left(\frac{W x_s}{T_H} + K_1\right) - \sinh K_1\right\} \tag{A4}$$

while the angle at any points of catenary measured from the horizontal direction is expressed as

$$\theta_s = \tan^{-1}\left\{\sinh\left(\frac{W x_s}{T_H} + K_1\right)\right\} \tag{A5}$$

In this study, the arc-length coordinate (s_s) is utilized as an independent variable. Therefore, from Eqs. (A1)-(A4), the vertical and horizontal coordinates of catenary can be rewritten with some manipulations as

$$y_s = \frac{T_H}{W}\left\{\cosh\left[\sinh^{-1}\left(\frac{W s_s}{T_H} + \sinh K_1\right)\right]\right\} + K_2 \tag{A6}$$

$$x_s = \frac{T_H}{W}\left[\sinh^{-1}\left(\frac{W s_s}{T_H} + \sinh K_1\right) - K_1\right] \tag{A7}$$

From Eqs. (A5) and (A7), the angle along the length of catenary measured along the arc-length of the catenary is written as

$$\theta_s = \tan^{-1}\left\{\sinh\left[\sinh^{-1}\left(\frac{W s_s}{T_H} + \sinh K_1\right)\right]\right\} \tag{A8}$$

It is well known that, in case of catenary, the horizontal tension component is constant along the length; therefore the axial tension force at any points of the catenary (see Fig. 1(b)) is simply calculated by

$$T_s = T_H \sec\theta_s \tag{A9}$$

To find the catenary solution, the total catenary length (S), the water depth (Y_H), and the horizontal top tension (T_H) are specified, while the horizontal offset (X_H)is solved numerically by applying the Newton iterative scheme to Eq. (A4). Then, the unknown parameters K_1 and K_2 can be calculated, and the catenary configuration is later obtained.